Transition from saltation to collisional regime in wind-blown sand: Supplementary material

J-L. Ralaiarisoa[1,5], J-B. Besnard[1,2], B. Furieri[3], P. Dupont[2], A. Ould El Moctar[4], F. Naaim-Bouvet[5], A. Valance[1]
[1] *Univ Rennes, CNRS, Institut de Physique de Rennes, UMR 6251, 3500 Rennes, France*
[2] *Univ Rennes, INSA Rennes, LGCGM, 3500 Rennes, France*
[3] *Universidade Federal do Espírito Santo, DEA, 29060-970 Vitória, ES, Brazil*
[4] *Univ Nantes, Laboratoire Thermique et Energie, UMR 6607, 44306 Nantes Cedex, France*
[5] *Univ. Grenoble Alpes, INRAE, UR ETNA, 38000 Grenoble, France*
(Dated: April 20, 2020)

In this supplement, we provide further details concerning the experimental measurements and and the discrete simulations.

I. WIND-TUNNEL MEASUREMENTS

A. Sand feactures

We used quartz sand with a mean diameter $d \approx 190\,\mu m$ (see Fig. 1). The values for d_{10} and d_{90} are 105 and $300\,\mu m$, respectively. It is important to note that in the discrete simulations we employ an uniform particle size distribution with a much narrower width (i.e., $d \pm 10\,\%$).

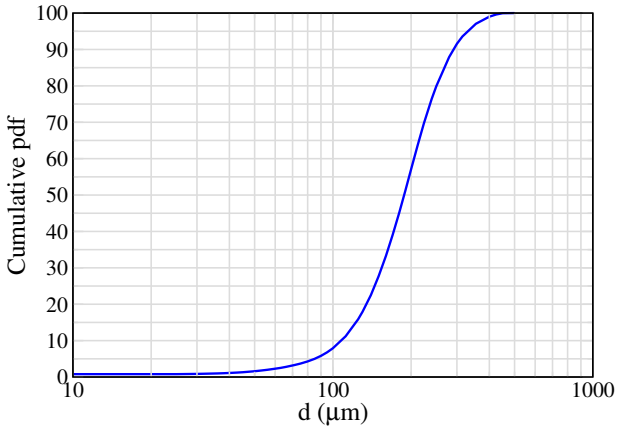

Figure 1: Cumulative particle size distribution of the sand used in the experiments obtained by laser diffractometry.

B. Tunnel dimensions

Our wind-tunnel is $6\,m$ long and has a $0.27\,m \times 0.27\,m$ cross-section. The finite dimensions of the wind tunnel can influence the boundary layer and the sand transport features.

The first requirement is that the tunnel should be long enough to achieve a steady and fully-developed state of transport. In our experiments, we checked that from Shields number up to $S^* = 0.3$ (i.e., in the saltation regime), the flow is steady and fully-developed after a downstream distance less than $2m$ [1]. In the collisional regime (i.e., for Shields number from 0.3 to 1), we do not have any estimation of the length necessary to achieve an equilibrium state of transport. It is likely that the equilibrium length increases and becomes greater than $2\,m$. However, we assume that the latter remains smaller than $6\,m$. The evolution of the equilibrium length with the wind speed in these high Shields number regime is definitively an interesting and open issue which would deserve detailed experimental studies.

Another important requirement concerns the tunnel height. We should take care that the tunnel is high enough to prevent the particles from colliding with the ceiling of the tunnel. In the saltation regime, the characteristic height of the transport layer is constant and of the order of $100\,d$, that is $2\,cm$ which is much smaller than tunnel height $H = 27cm$. In the collisional regime, the latter increases with increasing wind speed. It is increased by a factor 2 for the highest wind speed and approaches $4\,cm$ which remains again safely smaller than the tunnel height.

C. Side-wall effects on the mass flow rate

We find it worthwhile to detail how the mass flow rate is measured and corrected to get rid of the effect of side-walls. The mass flow rate Q provided in the article corresponds to the mass per unit mass and per unit width at the center of the tunnel, where we are free from the influence of the side-walls. The measurements of the mass flow rate Q at the center of the tunnel requires a selective sand trap system [2] which is able to collect and sort the grains according to their cross-wise position. In contrast, the assessment of the mass flow rate over the whole width of the tunnel is much simpler because it suffices to collect all the grains that exit the tunnel without selection. However, this measurement of the mass flow rate (called hereafter $< Q >$) is biased by the side-wall effects and is thus smaller than Q. There is therefore a correction factor if we want to infer the unbiased mass flow rate Q from the width-averaged mass flow rate $< Q >$. This correction is dependent of the tunnel width. For wide tunnels, the correction factor is expected to be close to 1 whereas for thin ones, the latter can be significantly

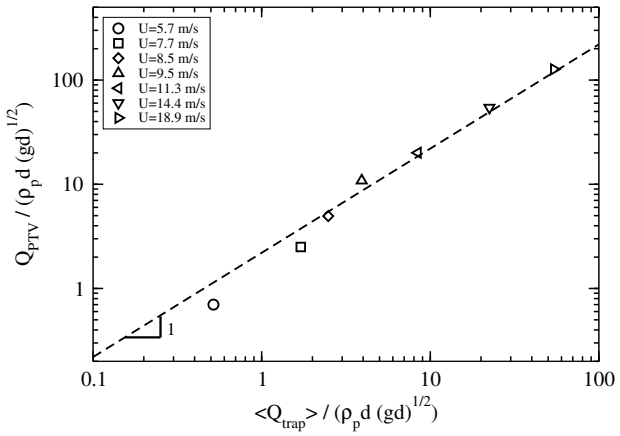

Figure 2: Comparison between the mass flow rate Q_{PTV} measured at the center of the tunnel by PTV techniques and the width-averaged mass flux $< Q >$ estimated by sand trap. Q_{PTV} remains fairly proportional to $< Q >$ over the entire range of investigated wind speed ($5\,m/s < U_\infty < 19\,m/s$)

greater than 1. This is the case for our wind-tunnel which has a relative small width $W = 0.27\,m$. We get a correction factor $Q/ < Q > \approx 2.3$ which is large but appears to be independent of the Shields number. This correction factor was determined up to Shields number $S^* = 0.2$ ($U_\infty \approx 9\,m/s$) [2] thanks to the selective sand trap system mentioned above. At higher Shields number, this device fails to capture efficiently the sand and an alternative method was employed to check the proportionality between Q and $< Q >$. The latter is based on Particle Tracking Velocimetry (PTV) techniques [3] and allowed to confirm that the correction factor remains fairly constant up to Shields number $S^* \approx 1.2$ ($U_\infty = 19m/s$) (see Fig. 2).

Importantly, the data of the mass flow rate Q presented in Fig. 1 come from measurements of the width-averaged mass flow rate $< Q >$ on which we applied the correction factor 2.3.

D. Experimental data

We provide here the tables displaying the experimental data from Figs. 1-4 of the paper, namely the mass flux versus the Shields number, the air and grain velocity profiles as well as the mass flux density profiles (see tables I-IV).

II. NUMERICAL SIMULATIONS

A. Implementation

We used the same approach as that developed by Duran et al. [4]. We thus only provide the main lines of the

S^*	$Q/(\rho_p d\sqrt{gd})$
0.056	1.26
0.163	4.07
0.203	5.98
0.274	9.40
0.325	13.60
0.368	20.28
0.498	34.15
0.633	53.82
0.930	91.74
1.234	129.90

Table I: Dimensionless mass flow rate data (i.e.,$Q/(\rho_p d\sqrt{gd})$) versus the Shields number.

$U_\infty = 5.1\,m/s$ $S^* = 0.034$		$U_\infty = 7.2\,m/s$ $S^* = 0.110$		$U_\infty = 9.2\,m/s$ $S^* = 0.215$		$U_\infty = 11.0\,m/s$ $S^* = 0.349$	
z (mm)	U (m/s)	z (mm)	U (m/s)	z (mm)	U (m/s)	z (mm)	U (m/s)
10.25	3.28	10.25	3.54	10.25	3.55	10.25	3.15
16.	3.77	16.	4.31	16.	4.66	16.	4.60
20.	4.05	20.	4.75	20.	5.29	20.	5.42
25.	4.24	25.25	4.88	25.25	5.48	25.25	5.75
29.75	4.38	29.75	5.12	30.	5.85	30	6.27
390.	4.75	392.5	5.74	39.25	6.68	39.25	7.38

$U_\infty = 12.9\,m/s$ $S^* = 0.520$		$U_\infty = 14.7\,m/s$ $S^* = 0.720$		$U_\infty = 16.7\,m/s$ $S^* = 0.933$		$U_\infty = 18.6\,m/s$ $S^* = 1.252$	
z (mm)	U (m/s)	z (mm)	U (m/s)	z (mm)	U (m/s)	z (mm)	U (m/s)
10.25	2.76	10.75	2.43	11.	2.01	11.25	1.92
16.	4.58	16.5	4.44	16.75	4.34	17.0	4.45
20.0	5.55	20.5	5.72	20.75	5.77	21.0	6.04
25.5	6.04	25.75	6.27	26.0	6.42	26.75	6.66
30.25	6.68	30.5	7.03	30.75	7.36	31.5	7.66
39.5	8.03	39.75	8.59	40.0	9.18	40.75	9.65

Table II: Air velocity profiles for various wind strengths.

S^*	0.034	0.108	0.152	0.217	0.348	0.668	1.302
z (mm)	u (m/s)						
1.14	0.49	0.61	0.69	0.90	1.14	1.61	2.02
9.14	1.34	1.56	1.69	1.85	2.11	2.75	3.28
17.14	1.91	2.37	2.59	2.85	3.18	3.98	4.57
25.14	2.24	2.98	3.29	3.66	4.07	5.13	5.92
33.14	2.49	3.53	3.84	4.39	4.84	6.13	7.21
41.14		3.90	4.31	4.95	5.54	7.08	8.40
49.14		4.02	4.62	5.46	6.11	7.92	9.48
57.14			4.78	5.82	6.63	8.68	10.45
65.14			4.86	6.06	7.03	9.36	11.32
73.14					7.36	9.94	12.09
81.14					7.49	10.45	12.81

Table III: Particle velocity profiles for various Shields number S^*.

S^*	0.056	0.164	0.275	0.37	0.5	0.934	1.64
z (mm)	q $(kg/m.s)$						
30	0.076	0.208	0.428	1.181	2.969		19.259
45	0.040	0.092	0.166	0.433	1.266	7.296	14.329
63	0.015	0.037	0.070	0.166	0.563	4.311	10.575
120	0.0006	0.0025	0.0056	0.012	0.074	0.659	3.104

Table IV: Flux density profiles for various Shields number S^*.

Normal spring stiffness k_n	2.10^5 (mg/d)
Normal restitution coefficient e_n	0.9
Normal damping coefficient γ_n	21.2 $(m\sqrt{g/d})$
Tangential damping coefficient γ_t	γ_n
Coulomb friction coefficient μ	0.5

Table V: Simulations parameters. The particles have a mean diameter $d = 0.2\,mm$ and a density $\rho_p = 2650\,kg/m^3$.

strategy together with the underlying physical hypotheses. The particle phase is described by a Lagrangian approach and each particle obeys the following equations in their dimensionless form:

$$\frac{d\vec{u^p}}{dt} = -\vec{e}_z + \sum_q \vec{f}_c^{p,q} + \vec{f}_{drag}^{p} \quad (1)$$

$$I\frac{d\vec{\omega^p}}{dt} = \frac{1}{2}\sum_q \vec{n}^{p,q} \times \vec{f}_c^{p,q} \quad (2)$$

where $\vec{f}_c^{p,q}$ stands for the contact forces and $\vec{f}_{drag}^{p} = D\left[(U-u^p)\vec{e}_x - v^p\vec{e}_z\right]$ is the air drag force with $D = (0.3\sqrt{(U-u^p)^2+v^{p2}}+18/R)/\sigma$ ($R = d\sqrt{(1-1/\sigma)gd}/\nu$ is the particle Reynolds number and $\sigma = \rho_p/\rho_{air}$ is the particle to air density ratio). Note that lengths, velocities and forces have been made dimensionless by the diameter d of the particle, $\sqrt{(1-1/\sigma)gd}$ and mg, respectively. The fluid phase is solved by a continuum description based on Reynolds average Navier-Stokes equations:

$$(1-\phi)D_t\vec{U} = (1-\phi)\sigma\left(-\vec{\nabla}p + 1/(\sigma-1)\vec{g} + \vec{\nabla}.\bar{\bar{\tau}}^f\right) - \sigma\vec{F} \quad (3)$$

with $\vec{F}(z) = \phi\langle\sum_{p\in[z;z+dz]}\vec{f}_{drag}^{p}\rangle/\langle\sum_{p\in[z;z+dz]}1\rangle$ and $\tau^f = (1/\sigma)\left(1/R + l^2|\partial_z U|\right)\partial_z U$ (where l is the Prandtl turbulent mixing length). F represents the average volume force exerted by the particles on the fluid and τ_f stands for the fluid shear stress. Note that as in [4], the mixing turbulent length is calculated using a differential equation that makes it vanish smoothly within the static bed.

The simulated system is two-dimensional with a stream-wise length $L = 500\,d$ and contains 8000 particles. Periodic boundary conditions are employed in the stream-wise direction. We used spherical particles with a polydispersity of $\pm 10\%$. Importantly, the system is not bounded in height.

The particle phase is modeled via discrete element methods. The particles consist of nondeformable spheres. Normal contact forces between interacting particles are modeled via a visco-elastic approach: $F_n = (k_n\delta + \gamma_n v_n)$, where δ is the overlap between the nondeformable spheres, v_n the normal component of the relative translational grain velocities, k_n the spring stiffness, and γ_n the viscous damping coefficient. Normal relative velocities before and after contact are related by a constant coefficient of normal restitution e_n. If the values of e_n and k_n are prescribed, γ_n is deduced from the following relation: $\gamma_n = m\sqrt{\frac{2k_n/m}{1+\pi^2/\ln(e_n)^2}}$. The tangential force F_t is described via a Coulomb friction model regularized through a viscous damping: $F_t = -min(\mu F_n, \gamma_s v_s)sign(v_s)$, where μ is the Coulomb friction coefficient, v_s the relative slip velocity at contact and γ_s the viscous damping coefficient. The values used for the parameters k_n, γ_n, γ_s and μ are reported in the table V

B. Bed surface and depth-averaged quantities

To assess quantities at the bed surface, it is necessary to define it. There is not a unique way to do it since the boundary between the static bed and the mobile layer is not a sharp interface. We define the bed surface as the height at which the volume fraction is half the maximum volume fraction $\phi = \phi_{max}/2$ as done in [4]. We use this definition to determine for example the mass flux density q_0 at the bed surface.

Depth-averaged quantities can be very sensitive to the definition chosen for the bed surface. To circumvent this difficulty, we employ depth-averaging procedure which are independent of the bed surface definition. In particular, we define the depth-integrated particle concentration M (called also the mass hold-up) and the depth-averaged particle velocity $< u >$ as done in [4]:

$$M = \frac{\left(\sum_i u_i\right)^2}{A\sum_i u_i^2} \quad (4)$$

$$< u > = \frac{\sum_i u_i^2}{\sum_i u_i} \quad (5)$$

where A is the horizontal surface extent of the simulation domain (i.e., $500d \times 1d$) and the sum is done over all particles (static or mobile). With these definitions, the mass flow rate is simply the product of the mass hold-up and depth-averaged velocity: $Q = M \times < u >$.

As an example, we show in Fig. 3 the evolution of the mass hold-up with the Shields number.

C. Mean free path

We detail below the method we used to calculate the mean free path. As the system is heterogeneous, the

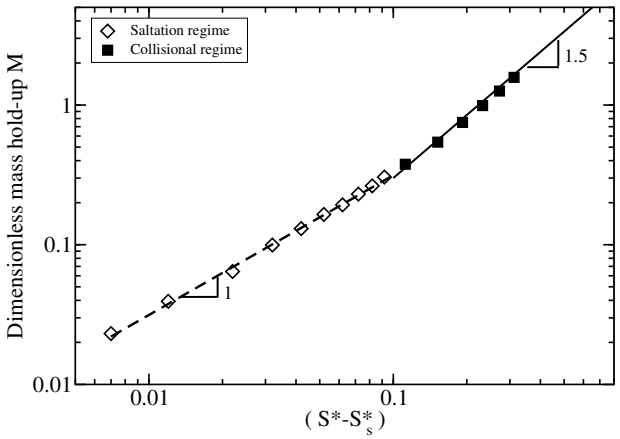

Figure 3: Dimensionless mass hold-up versus the Shields number. In the saltation regime, $M \propto (S^* - S_s^*)$ whereas in the collisional regime $M \propto S^{*1.5}$.

mean free path is expected to vary with the particle elevation. To calculate the mean free path, we do as follows. We decompose the motion of all mobile particles into successive hops and sort the hops into different subsets according to their maximum elevation height z_m within a given tolerance $\Delta z = \pm 1d$. For a given subset, we determine the elevation at which they undergo a collision both in the ascent and descent part of their trajectory (z_i^a and z_i^d respectively) and define a mean free path $l(z_m)$ calculated as follows:

$$l(z_m) = (1/n) \sum_{subset\, i} \left[(z_m - z_i^a) + (z_m - z_i^d) \right] . \qquad (6)$$

With this definition, the mean free path $l(z_m)$ is simply related to the average elevation z_c at which the particles undergo a collision: $z_c = (< z_i^a + z_i^d >)/2 = 2z_m - l$. A mean free path equal to twice the maximum elevation gives $z_c = 0$ indicating that the particles collide with the static bed. A smaller mean free path indicates a collision that occurs above the static bed. In the figure 8 of the paper, we provide the mean free path for two different subsets of particles corresponding to a maximum elevation $z_m = 50d$ and $100d$, respectively.

[1] H. Selmani, A. Valance, A. Ould El Moctar, P. Dupont, and R. Zegadi *Geophysical Research Letters*, 45:1838–1844 (2018).

[2] T. D. Ho. *Phd Thesis, University of Rennes, France* , 2012.

[3] M. Creyssels, P. Dupont, A. Ould El Moctar, A. Valance, I. Cantat, J.T. Jenkins, J.M. Pasini, and K.R. Rasmussen. *Journal of Fluid Mechanics*, 625:47–74, 2009.

[4] O. Duran, B. Andreotti, and P. Claudin. *Phys. Fluids*, 24:103306, 2012.